Enhanced Thermoelectric Performance by Resonant Doping and Embedded Magnetic Impurity

Sujin Kim,[1] Junphil Hwang,[1,2,*] Tae-Soo You,[3] Seongbeom Yeon,[3] Jungwon Kim,[4] Byung-Kyu Yu,[1] Mi-Kyung Han,[1] Minju Lee,[1] Somnath Acharya,[5] Jiyong Kim,[5] Woochul Kim,[5] and Sung-Jin Kim[1,†]

[1] *Department of Chemistry and Nano Science, Ewha Womans University, Seoul 120-750, Korea*

[2] *Green Energy R&D Division, Korea Construction Equipment Technology Institute (KOCETI), Jeonbuk 54004, Korea*

[3] *Department of Chemistry and BK21 Four Research Team, Chungbuk National University, Cheongju, Chungbuk 28644, Korea*

[4] *Institute of Advanced Composite Materials, Korea Institute of Science and Technology (KIST), Jeonbuk 55324, Korea*

[5] *School of Mechanical Engineering, Yonsei University, Seoul 120-749, Korea*

(Received 4 April 2022; revised 8 November 2022; accepted 28 November 2022; published 11 January 2023)

The thermoelectric energy-conversion efficiency is significantly enhanced by introducing magnetism. Doping Cr atoms in a Cu_2SnS_3(CTS) matrix modifies the electron density of state (*e*-DOS) and causes a special electron-transport mechanism by localized impurity spin moments. The localized spin moments cause a spin-spin exchange interaction with the spin of itinerant electrons of the CTS matrix. This is clearly verified in *M*-*T* measurement, which deviated from Curie's law. The figure of merit (zT) of the magnetic nanocomposite was 8 times higher than that of pristine CTS by the synergetic effect of modifying *e*-DOS near the Fermi level and electron transport by localized spin moments.

DOI: 10.1103/PhysRevApplied.19.014034

I. INTRODUCTION

Introducing magnetism into thermoelectric materials is an alternative strategy to enhance the performance of thermoelectric energy conversion. Thermoelectric material can convert heat into electricity directly and vice versa, and these materials have received attention in recent years due to their potential applications in power generation and cooling systems [1]. Thermoelectric energy-conversion efficiency is related to the dimensionless parameter, thermoelectric figure of merit $zT(=S^2\sigma T/\kappa_{\text{tot}})$ where S is the Seebeck coefficient, σ is the electrical conductivity, κ is the thermal conductivity, and T is the absolute temperature. $S^2\sigma$ is called the power factor, and the total thermal conductivity can be expressed as $\kappa_{\text{tot}} = \kappa_e + \kappa_L$ [2,3]. Enhancement of zT is challenging because of the adverse coupling of each parameter [2]. Particularly for power factor ($S^2\sigma$), the S and σ are inversely interdependent [2].

$$S = \frac{1}{eT}\frac{\int_0^\infty E\tau(E)(E-E_F)D(E)(\partial f/\partial E)dE}{\int_0^\infty E\tau(E)D(E)(\partial f/\partial E)dE}. \quad (1)$$

Here, E is electron energy, D is density of states, f is Fermi-Dirac distribution, and τ is scattering time. The denominator of Eq. (1) is the σ, therefore, to decouple the S and σ, it is necessary to modify the energy dependence of the integrand in the numerator; particularly the electron density of states (*e*-DOS) and scattering time (τ) of carriers [2,4]. Modifying *e*-DOS is carried out by doping resonant dopant [5–16]. The resonant dopant could change the slope of the $D(E)$ near the Fermi level resulting in decoupling of S and σ. Recently, magnetism-related thermoelectricity has appeared as a powerful strategy to decouple the S and σ, resulting in an enhanced power factor. In magnetic materials, the magnon-drag Seebeck effect has been widely studied previously [17–20]. The quantized spin current in a magnetic material is called a magnon, which causes drag of itinerant electrons. Therefore, this mechanism is limited for magnetic materials, such as ferromagnetic (FM), antiferromagnetic (AFM), or paramagnetic (PM) materials. The contribution of magnon drag to the Seebeck coefficient is quite large in magnetic materials [18]. However, most of the widely studied thermoelectric materials are diamagnetic (DM). Recently, studies of thermoelectric materials containing magnetic impurities in a DM matrix were reported. The first example is the magnetic nanoparticles' embedded nanocomposite. Zhao's group reported nanocomposites consisting of embedded superparamagnetic (SPM) nanoparticles (NPs) in a DM bulk thermoelectric matrix [21–24]. They suggested that localized spin-angular-momentum fluctuations due to SPM NPs

*tainm7@naver.com
†sjkim@ewha.ac.kr

affect itinerant electron transport, a phenomenon called "multiple scattering" [21,22]. The fluctuation of spin angular momentum of SPM NP is called a "Neel relaxation", as expressed by Eq. (2) [25]:

$$\tau_N = \tau_0 exp\left(\frac{KV}{k_B T}\right). \tag{2}$$

Here, τ_N is the Neel-relaxation time, τ_0 is the time constant, which is on the order of a few nanoseconds, K is the anisotropy energy per unit volume, V is the nanoparticle volume, k_B is the Boltzmann constant, and T is the absolute temperature [25]. Zhao suggested that the correlation between itinerant electrons and the Neel relaxation could enhance the Seebeck coefficient, because it changes the electron-scattering mechanism, resulting in an increase of scattering parameter, r, where, $\tau = \tau_0 E^r$ [21,22]. The second example is the atomic impurity by magnetic dopants. Several studies reported various DM thermoelectric materials doped with magnetic atoms with unfilled d orbital, such as Fe, Co, Ni, Cr, and Mn etc. [26–33]. There were unusual enhancements of Seebeck coefficients in such alloys and the results [14–21] suggested that the localized spin moment in atomic impurities could affect itinerant electrons, which is similar to the Kondo effect [21,34,35]. The Kondo effect occurs in solid solution containing magnetic impurity in nonmagnetic matrix. The theory described the interaction between localized spin of d orbital in impurity atom and spin of itinerant electron of s orbital in the matrix [34]. However, in the thermoelectric field, the spin-spin exchange interaction was not fully discussed and direct evidences of exchange interaction were not clarified. In this work, we select Cu_2SnS_3 (CTS) as a matrix material, because it can be a potential candidate for ecofriendly thermoelectric materials [36–41]. This material has been studied in thermoelectric field with the various dopant [24–31]. Also, the change of Cu/Sn ratio induced the modification of lattice symmetry resulting in various crystal structure [42–44]. Here, we prepare the Cr-doped CTS with monoclinic phase, where around 5% of Cr atoms substituted on the Sn site and the additional amount of Cr is precipitated as nanosized SPM-$CuCrSnS_4$ particles.

II. MAGNETIC AND ELECTRONIC PROPERTIES

The nanostructure of SPM-$CuCrSnS_4$ is confirmed in TEM study, which is shown in Figs. 1, S1 and S2 within the Supplemental Material [45]. The change of lattice parameters shown in Fig. S3 within the Supplemental Material [45,56,57] indicates that only 5 at.% of Cr is substituted into Sn sites and the additional amount of Cr made the precipitate of $CuCrSnS_4$ as a secondary phase. In various doping concentrations, the x% of Cr-doped-Cu_2SnS_3 with magnetic $CuCrSnS_4$ nanoprecipitates is referred to as "CTS-Cr x%-MNC", where "CTS" refers to copper-tin-sulfide, Cu_2SnS_3, and "MNC" refers to a magnetic nanocomposite. A schematic model for spin-spin exchange interaction between localized spin moments of magnetic impurities and spin of itinerant electrons in matrix CTS is shown in Fig. 1(a). In CTS-Cr x%-MNCs, there are two types of localized spin moments by SPM-$CuCrSnS_4$-NPs and substituted Cr atoms. The two types of localized spin moments have different relaxational dynamics at high temperature, which are called Neel relaxation [25] of SPM-$CuCrSnS_4$ nanoprecipitates and Korringa relaxation [58] of substituted Cr atom. They induce spin-spin exchange interactions with spin of itinerant electrons in matrix CTS because of antiferromagnetic coupling [21,34,35,58–60]. The interaction between spin moments of SPM NP and itinerant electron is called "multiple scattering" by Zhao [21]. Meanwhile, the interaction between the spin of localized magnetic dopant (electrons in the d orbital of localized Cr atom) and the itinerant electron of matrix CTS (electrons in s orbital of matrix CTS) is called "s-d exchange interaction," especially "Kondo effect" at low temperature, described by Anderson Hamiltonian [59,60]. The CTS-Cr 15%-MNC sample shows a slight deviation from linearity in the $1/\chi$ plot as a function of temperature just above the AFM-SPM-transition, as highlighted in Fig. 1(c). This is observed in low temperature, however, it is an indication of the spin-spin exchange interaction due to the following reasons. Generally in the PM regime, the magnetic susceptibility (χ) should follow Curie's law as shown in the following equation [61]:

$$\chi = \frac{M}{H} = \frac{g^2 S(S+1)\mu_B}{3k_B T} = \frac{C}{T}. \tag{3}$$

Here, M is magnetization, H is an applied magnetic field, g is the Lande g factor, S is spin angular momentum, and μ_B is the Bohr magneton. Therefore, in the PM regime, the $1/\chi$ versus temperature should show a linear dependence. However, when there a spin-spin exchange interaction, the temperature dependence of $1/\chi$ can be changed. The first theoretical explanation about the spin-spin exchange interaction was studied by Kondo [34,35]. The magnetic susceptibility under spin-spin exchange interaction (s-d interaction) could be described based on the following equation [60]:

$$\chi = \frac{C}{T}\left[1 + \frac{J \times D}{N}\left(1 - \frac{J \times D}{N}\log\frac{k_B T}{E_D}\right)^{-1}\right]. \tag{4}$$

Here, J is the exchange-interaction constant, D is the density of states at the Fermi energy, N is the atom number density, and E_D is the band width. As shown in Eq. (4), the temperature dependence of $1/\chi$ is nonlinear when there is the spin-spin exchange interaction. After the Kondo

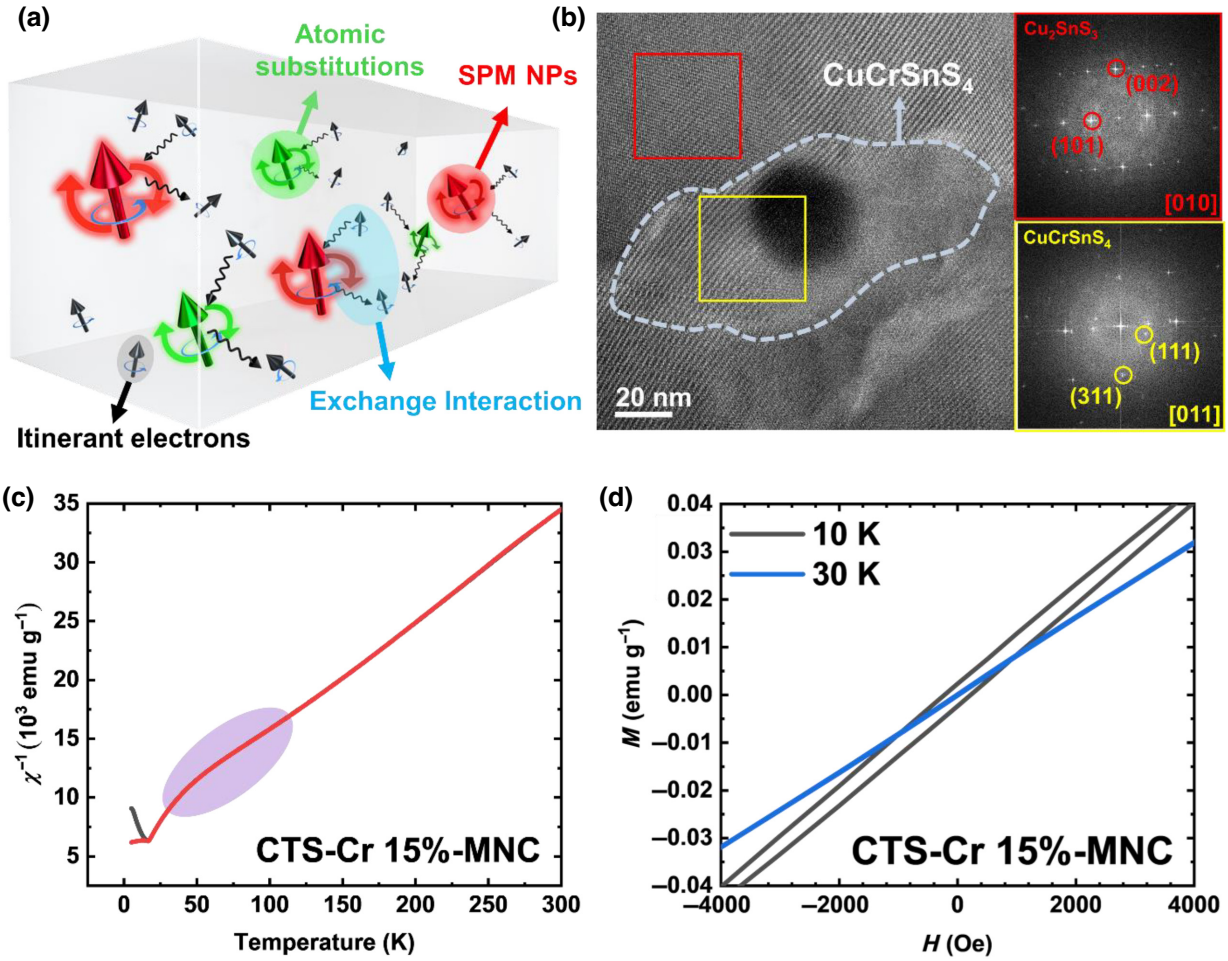

FIG. 1. (a) Schematic of exchange-interaction between localized spin moments (SPM-$CuCrSnS_4$-NPs and atomic substitution of Cr atom) and spin of itinerant electrons in the CTS matrix. (b) High-resolution TEM image for $CuCrSnS_4$ superparamagnetic nanoprecipitates. (c) Temperature dependence of magnetic susceptibility. The highlighted region indicates a general feature of Kondo-like behavior, which means there is the exchange interaction between two spins (impurity and itinerant electron). (d) Magnetic hysteresis loop for CTS-Cr 15%-MNC.

effect was reported, a more advanced theoretical description using numerical renormalization group theory was reported by Wilson [59]. The nonlinear feature of $1/\chi$ versus T in Kondo alloy at low temperature was also confirmed in experiments [62]. Because of the thermal fluctuation at high temperature, the effect of exchange interaction to magnetic susceptibility is only observed at low temperature. In our CTS-Cr x%-MNC($x = 0,5,10,15,20$), both precipitated SPM NPs and substituted Cr atoms acted as localized spin moments in the DM-CTS matrix, resulting AFM SPM behavior of magnetic susceptibility (χ) as shown in Fig. S6 within the Supplemental Material [45]. The pristine CTS indicates clear DM behavior, whereas the CTS-Cr 15%-MNC shows AFM SPM transition behavior at the blocking temperature around $T_B = 17$ K. Below 17 K, the magnetization of the sample shows different values for zero-field-cooling (ZFC) and field-cooling (FC) measurements, which is the general behavior of the AFM regime. Above 17 K, the magnetization shows PM behavior following Curie's law. However, as mentioned in the earlier section, there was a slight deviation from Curie's law as shown in Fig. 1(c). The spinel $CuCrSnS_4$ has AFM behavior whose Neel temperature is around 10–20 K, which is consistent with our results [63,64]. Therefore, it is clear that the AFM SPM behavior of CTS-Cr 15%-MNC originated dominantly from the nanoprecipitate of the spinel $CuCrSnS_4$ phase. The M-H hysteresis curve is obtained at 10 and 30 K, considering $T_B = 17$ K as plotted on Fig. 1(d). The hysteresis loop is open below the T_B and closed above it, which indicates an AFM SPM transition.

The Seebeck coefficients of CTS-Cr x%-MNC ($x = 10,15,20$) are reduced, and that of CTS-Cr 5%-MNC is enhanced comparing pristine CTS as plotted in Fig. 2(a). However, the reductions of Seebeck coefficients in CTS-Cr x%-MNC($x = 10,15,20$) are not significant considering the large enhancement of carrier concentration

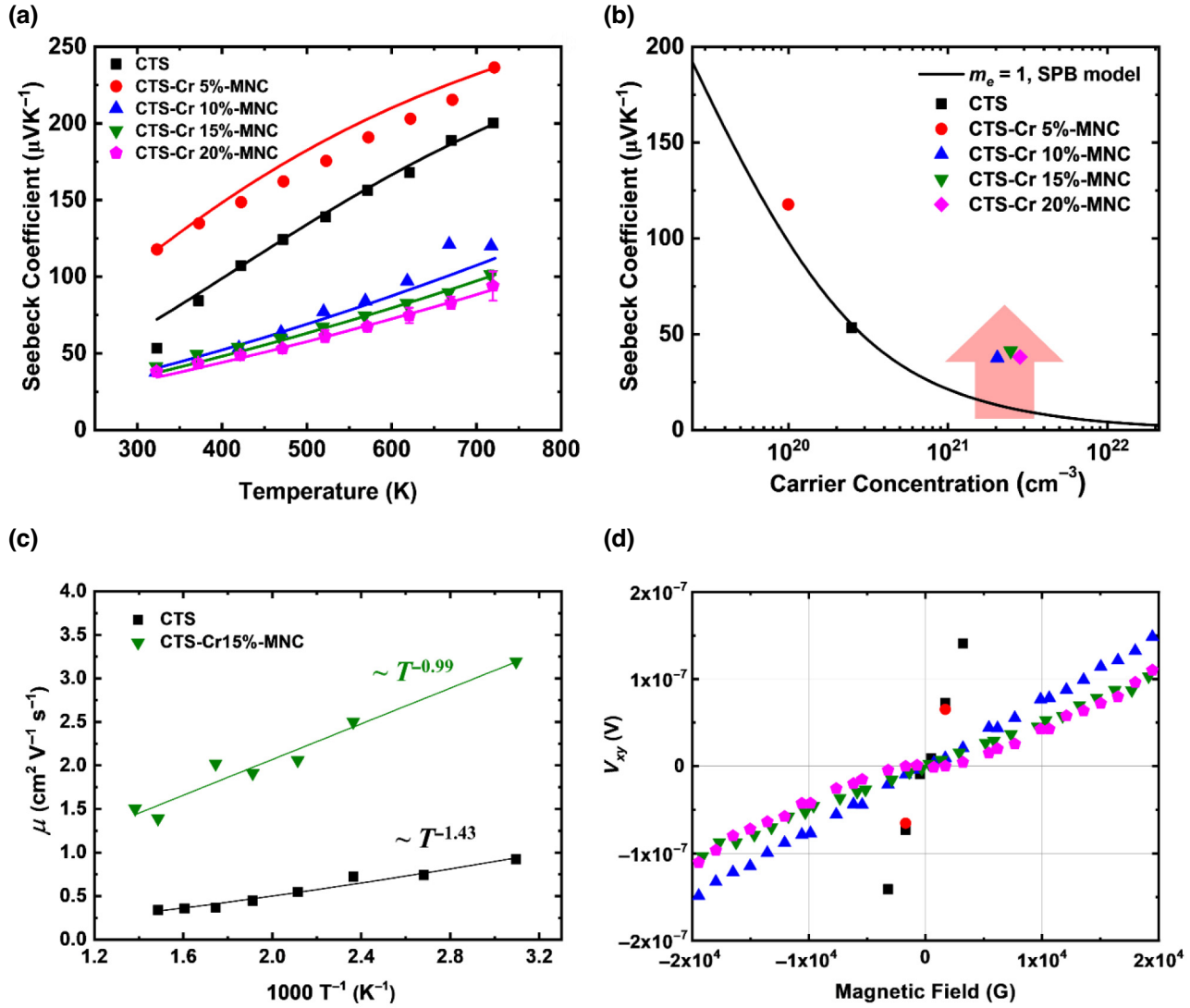

FIG. 2. (a) Temperature-dependent Seebeck coefficient. (b) Pisarenko plot. (c) Temperature-dependent mobility. (d) Field-dependent Hall voltage (V_{xy}). Anomalous Hall effect is observed in CTS-Cr 20%-MNC.

(approximately 10 times that of pure CTS). The Pisarenko plot showing a correlation between Seebeck coefficient and carrier concentration is plotted in Fig. 2(b). The CTS-Cr x%-MNC($x = 10,15,20$) samples had higher Seebeck coefficients than theoretically estimated values with the single-parabolic-band model [65].

$$S = \frac{k_B}{e}\left[\frac{(r+(5/2))F_{r+(3/2)}(\eta)}{(r+(3/2))F_{r+(1/2)}(\eta)} - \eta\right]. \qquad (5)$$

Here, F is the Fermi-Dirac integral, and η is the reduced Fermi level, E_F/k_BT. The enhancement of Seebeck coefficient in Fig. 2(b) could be explained by two synergetic effects: (1) the resonant doping of Cr; (2) change of electron-transport mechanism by spin-spin exchange interaction. We discuss the resonant doping of Cr using the density-functional theory (DFT) calculation results in the next section. To clarify the change of the transport mechanism, the temperature and field-dependent Hall-effect measurements are conducted as plotted on Figs. 2(c) and 2(d). The Seebeck enhancement by magnetic impurity has been discussed by Zhao's works [21,22], changing scattering parameters in Eq. (5) to fit the experimental data. However, there is no precise theoretical transport model to describe the spin-spin exchange interaction by localized SPM NPs. Moreover, in our sample, the effective mass also could be changed by resonant Cr doping. Therefore, the quantitative analysis of the Seebeck coefficient of our samples is inaccurate. However, the anomaly in Hall-effect measurements in Figs. 2(c) and 2(d) still confirms the change of electron transport by localized spin moment. The pristine CTS sample shows the dependence of $\mu \sim T^{-1.43}$, which is almost the same with acoustic phonon scattering dominant, $\mu \sim T^{-1.5}$ [65,66]. However, the CTS-Cr15%-MNC shows

the dependence of $\mu \sim T^{-0.99}$. This is the critical indication that the electron transport mechanism is changed in CTS-Cr15%-MNC due to localized spin moment of impurity $CuCrSnS_4$. The field-dependent Hall voltage shows anomalous Hall effect (AHE) for CTS-Cr20%-MNC as shown in Fig. 2(d). The field-dependent Hall-effect measurement is conducted at room temperature. The anomaly is the evidence of the localized spin moment of magnetic impurity affects to conduction electron [21–33]. The other MNC samples do not show the AHE because of thermal fluctuation in the paramagnetic region. The evidence of resonant doping of Cr is clarified using DFT calculation, which is discussed in the next section.

Figure 3 shows the electrical conductivities, carrier concentrations, and mobilities of CTS-Cr x%-MNC($x = 0,5,10,15,20$) and the result of e-DOS calculation based on DFT. The electrical conductivity increased to approximately 2000 S cm^{-1} at CTS-Cr 20%-MNC as shown in Fig. 3(a). They have metallic behavior, which is a general trend in heavily doped semiconductors. To clarify the enhancement of electrical conductivity, the carrier concentrations n and mobilities μ for our samples are obtained by Hall measurement as plotted in Fig. 3(b). The carrier concentration increases from 2.49×10^{20} cm^{-3}($x = 0$) to 2.82×10^{21} cm^{-3}($x = 20$), and the mobility of CTS-Cr x%-MNC($x = 0,5,10,15,20$) is also enhanced depending on Cr-doping concentration. Thus, enhanced electrical conductivity is caused by the increase of the carrier concentration and mobility. DFT calculation is conducted to clarify the reason of carrier-concentration enhancement. The e-DOS of Cr-doped CTS and the contribution of each element on total DOS are plotted in Fig. 3(c). The Sn orbitals only contribute to the upper conduction bands and the lower valence bands, which means they have little contribution to the states near the Fermi level. Sn orbitals provide electrons to saturate the chemical bonds and stabilize the compounds [67,68]. For this reason, doping the unfilled d-orbital atoms to Sn sites can change the electronic structure around the Fermi level and can increase the carrier concentration. The large enhancement of carrier concentration in Cr-doped-CTS samples could be caused by the electrons of Cr d orbital to the e-DOS near the Fermi level. The mobility of CTS-Cr x%-MNC($x = 10,15,20$) is also increased from pristine CTS, which is very interesting because they have more impurities than pristine CTS resulting in more electron scattering. The mobility is a function of scattering time and effective mass. The effective mass of CTS-Cr x%-MNC($x = 10,15,20$) must be increased because they have a resonant state near the Fermi level [61].

$$\mu = \frac{e\tau}{m},\ D(E) = \frac{1}{2\pi^2}\left(\frac{2m}{\hbar^2}\right)^{3/2}(E - E_c)^{1/2}. \quad (6)$$

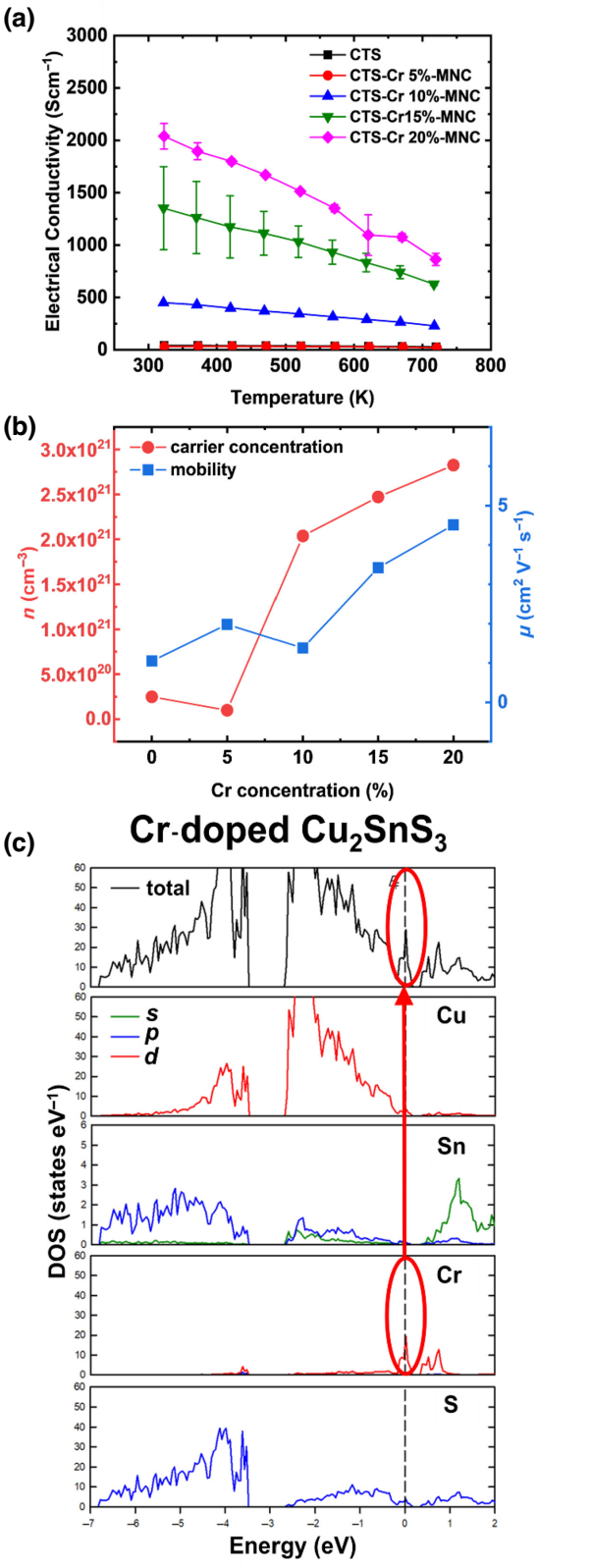

FIG. 3. (a) Electrical conductivities, (b) carrier concentration and mobility for CTS-Cr x %-MNC($x = 0,5,10,15,20$). (c) Results of e-DOS calculation for Cr-doped Cu_2SnS_3. The black line indicates total DOS, the red line is the contribution of the d orbital, blue is p, and the green is s.

Therefore, the scattering time of CTS-Cr x%-MNC ($x = 10,15,20$) will be much longer than pristine CTS considering the increased mobility in Fig. 3(c). Assuming there is no spin-spin exchange interaction and only impurity scattering happens, it is impossible to explain this increase of scattering time, because in CTS MNC, more impurities are distributed than pristine CTS. Therefore, the special transport phenomenon might happen in CTS MNC by spin-spin interaction. Further analysis could be carried out in future work. The temperature-dependent power factors of CTS-Cr x%-MNC($x = 0,5,10,15,20$) are plotted on Fig. 4(a). The power factor increases by approximately 520% compared with that of pristine CTS because of the large enhancement of electrical conductivity and a relatively small reduction of Seebeck coefficient in CTS-Cr x%-MNC($x = 10,15,20$) samples. The small reduction of Seebeck coefficient is expected due to the synergetic effect by resonant Cr doping and exchange interaction between localized spin moments and the spin of itinerant electrons. As described in Eq. (1) in the Introduction, the modification of the electron density of states and scattering time could decouple the Seebeck coefficient and electrical conductivity. The poor coupling of two electrical parameters limits the enhancement of thermoelectric energy conversion. By adding Cr in the CTS system, the energy dependence of e-DOS and scattering time could be modified effectively, resulting in huge enhancement of power factors. As shown in Fig. 4(b), the enhancement of power factor in CTS MNCs is outstanding compared to other SPM-NP-embedded nanocomposites [21–24,69]. In previously reported nanocomposites, only the magnetic NPs are embedded in the DM matrix, whereas our CTS-Cr-doped-MNCs have resonant state near the Fermi level and embedded magnetic NPs simultaneously by doping the Cr atom. The synergetic modification of e-DOS and scattering time significantly enhanced power factor by decoupling electrical conductivity and Seebeck coefficient.

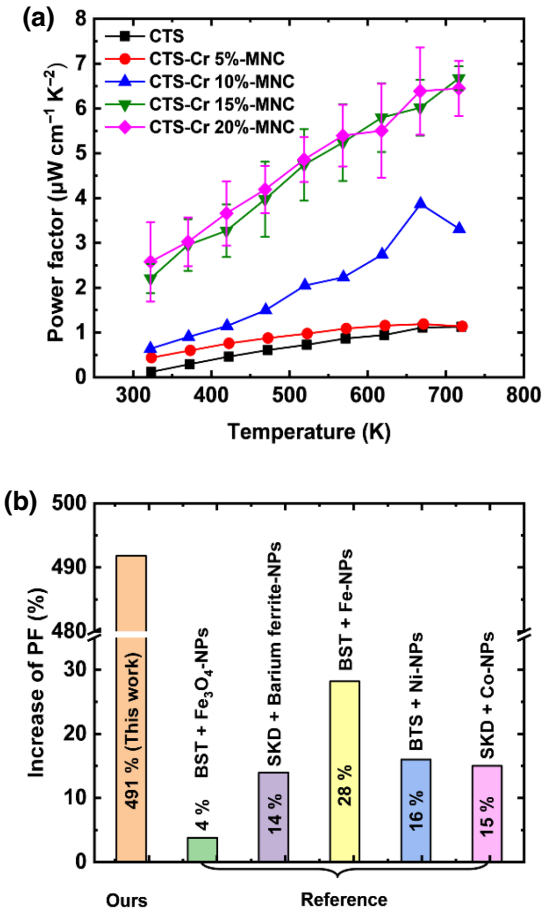

FIG. 4. (a) Power factors of CTS-Cr x%-MNC($x = 0,5,10,15,20$). (b) Comparison of power-factor enhancements with other SPM-NP-embedded nanocomposites [21–24,69]. The abbreviations are as follows: BST, Bi-Sb-Te alloy; SKD, Skutterudite; BST, Bi-Te-Se alloy.

III. THERMAL AND THERMOELECTRIC FIGURE OF MERITS

The thermal properties and thermoelectric figure of merit of CTS-Cr x%-MNC($x = 0,5,10,15,20$) are shown in Fig. 5. The total thermal conductivity decreased by Cr addition until $x = 15$. The thermal conductivity reductions of CTS-Cr x%-MNC($x = 5,10,15,20$) can be explained by bond softening due to Cr doping and phonon scattering by nanoparticles of $CuCrSnS_4$ and Cu_2S. According to the electron-localization-function (ELF) diagram shown in Fig. S8 within the Supplemental Material [45,46–53], the strong interatomic interactions between cation and S in the [SnS_4] tetrahedron decreased when Cr substituted Sn. Moreover, as shown in Table S2 within the Supplemental Material [45], the integrated-crystal-orbital-Hamilton-population (ICOHP) values in the Cr-doped CTS also proved that the orbital population in the [SnS_4] tetrahedron decreased due to the Cr doping compared to that of pristine CTS. It is well known that the chemical bond softening, also called phonon softening, enhances the anharmonicity of crystal (Grüneisen parameter) resulting in enhanced Umklapp scattering, and reduced phonon group velocity, thus reducing lattice thermal conductivity [69–73]. Theoretical lattice thermal conductivity could be calculated by changing the Grüneisen parameter (γ) using the Callaway model as plotted in Fig. S7 within the Supplemental Material [45,54,55]. The results in Fig. S7 within the Supplemental Material [45] show that the Grüneisen parameter (γ) in the CTS-Cr 15%-MNC sample increased to be around 2 times larger than that of pristine CTS. The value of $\gamma = 2.3$ is similar with that of PbTe($\gamma = 2.2$), which is an indication of strong phonon softening by resonant bonding of Pb—Te. It is noteworthy that CTS could have high γ without any heavy elements. The quantitative analysis

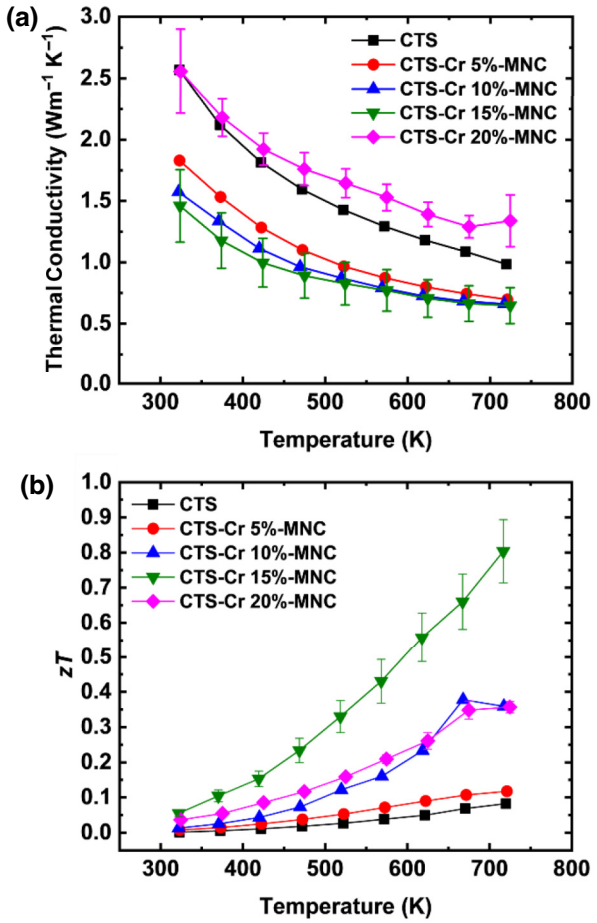

FIG. 5. Temperature-dependent (a) thermal conductivities, (b) thermoelectric figure of merit (zT).

of γ using the Callaway model is not a perfect estimation for our composite, because there might be other effects of phonon scattering by embedded nanoparticles of $CuCrSnS_4$ and Cu_2S, and the Lorenz number might be overestimated. However, the ELF diagram and ICOHP results show the chemical bonding could be softened by Cr substitution in the Sn site. The estimation of lattice thermal conductivity reduction considering phonon softening in Fig. S7 within the Supplemental Material [45] is in good agreement with experiments. Therefore, we conclude that the phonon softening by Cr substitution on the Sn site is the main reason of the lattice thermal conductivity reduction in CTS-Cr x%-MNC($x = 5,10,15,20$) samples. The thermoelectric figures of merit zT of the CTS-Cr x%-MNC($x = 0,5,10,15,20$) are shown in Fig. 5(b). The optimum doping amount of Cr is 15%, which showed $zT = 0.8$ at 723 K. The zT is significantly enhanced, approximately 8 times higher than $zT = 0.1$ of the pure CTS sample. This significant enhancement might be induced by synergetic effect of Cr substitution and the precipitation of SPM-$CuCrSnS_4$-NPs. The substituted Cr atom at the Sn site effectively modulates the e-DOS and increases the electrical conductivity significantly. The addition of Cr over solubility limit approximately 5% in CTS results in precipitation of SPM-$CuCrSnS_4$-NPs. The resonant doping Cr and spin-spin exchange interaction successfully decouple electrical conductivity and Seebeck coefficient, thus enhancing power factor. Also, the substitution of Cr in the Sn site of CTS could soften the phonon mode, effectively reducing lattice thermal conductivity. Thus, the synergetic effect of Cr addition in the CTS system caused a huge enhancement of thermoelectric energy-conversion performance. This is a very promising result because the CTS is an alternative thermoelectric material consisted of cheap, nontoxic elements.

IV. CONCLUSIONS

In summary, a magnetic nanocomposite consisted of Cr substitution in the CTS matrix and $CuCrSnS_4$ SPM nanoprecipitates is synthesized. The Cr substitution on the Sn site in CTS effectively modified the e-DOS. The existence of magnetic $CuCrSnS_4$ SPM NP in the CTS matrix induced alternative electron transport features by localized spin moments in the CTS matrix. The anomaly of the M-T graph, Hall-effect measurements provided direct evidence of exchange interaction between localized SPM spin moments and spins of itinerant electrons in the matrix. The additional scattering caused by such spin-spin exchange interaction minimizes the reduction of Seebeck coefficient despite increased carrier concentration. Because of the synergetic effect of Cr substitution and precipitated SPM NPs, a high power factor of 7 μW cm^{-1} K^{-2} is achieved in CTS-Cr 15%-MNC by decoupling of electrical parameters. The results of DFT calculation indicate that Cr substitution on Sn site in CTS also reduces thermal conductivity by phonon softening. The estimated Grüneisen parameter approximately 2.3 is similar to that of PbTe. The maximum zT value of 0.8 at 723 K in CTS-Cr 15%-MNC is 8 times higher than that of pristine CTS. The significant enhancement of the zT value is driven by the synergetic effect of spin-spin exchange interaction, e-DOS modification and phonon softening. This report suggests an alternative strategy for promising thermoelectric materials consisting of cheap and nontoxic elements through introducing magnetism.

ACKNOWLEDGMENTS

This research is supported by the Pioneer Research Center Program through the National Research Foundation of Korea (NRF) funded by the Ministry of Science, ICT & Future Planning (2022M3C1A309198811). This research is supported by Basic Science Research Program through the National Research Foundation of Korea (NRF) funded by the Ministry of Education (2021R1I1A1A01058838), and Basic Science Research Program through the National

Research Foundation of Korea (NRF) funded by the Ministry of Education (2021R1A6A1A10039823).

[1] D. M. Rowe, *CRC Handbook of Thermoelectrics* (CRC Press, Florida, 1995).

[2] G. Chen, *Nanoscale Energy Transport and Conversion* (Oxford University Press, New York, 2005).

[3] W. Kim, Vol. Ph.D., Thesis, University of California, Berkeley, 2005.

[4] A. M. Dehkordi, M. Zebarjadi, J. He, and T. M. Tritt, Thermoelectric power factor: Enhancement mechanisms and strategies for higher performance thermoelectric materials, Mater. Sci. Eng., R **97**, 1 (2015).

[5] J. P. Heremans, B. Wiendlocha, and A. M. Chamoire, Resonant levels in bulk thermoelectric semiconductors, Energy Environ. Sci. **5**, 5510 (2012).

[6] R. Al Rahal Al Orabi, N. A. Mecholsky, J. Hwang, W. Kim, J. S. Rhyee, D. Wee, and M. Fornari, Band degeneracy, low thermal conductivity, and high thermoelectric figure of merit in SnTe-CaTe alloys, Chem. Mater. **28**, 376 (2016).

[7] B. Wiendlocha, Fermi surface and electron dispersion of PbTe doped with resonant TI impurity from KKR-CPA calculations, Phys. Rev. B **88**, 205205 (2013).

[8] B. Wiendlocha, Thermopower of thermoelectric materials with resonant levels: PbTe:TI versus PbTe:Na and $Cu_{1-x}Ni_x$, Phys. Rev. B **97**, 205203 (2018).

[9] C. M. Jaworski, B. Wiendlocha, V. Jovovic, and J. P. Heremans, Combining alloy scattering of phonons and resonant electronic levels to reach a high thermoelectric figure of merit in PbTeSe and PbTeS alloys, Energy Environ. Sci. **4**, 4155 (2011).

[10] Q. Zhang, B. Liao, Y. Lan, K. Lukas, W. Liu, K. Esfarjani, C. Opeil, D. Broido, G. Chen, and Z. Ren, High thermoelectric performance by resonant dopant indium in nanostructured SnTe, Proc. Natl. Acad. Sci. U. S. A. **110**, 13261 (2013).

[11] S. Misra, B. Wiendlocha, J. Tobola, F. Fesquet, A. Dauscher, B. Lenoir, and C. Candolfi, Band structure engineering in $Sn_{1.03}Te$ through an In-induced resonant level, J. Mater. Chem. C **8**, 977 (2020).

[12] C. M. Jaworski, V. Kulbachinskii, and J. P. Heremans, Resonant level formed by tin in Bi_2Te_3 and the enhancement of room-temperature thermoelectric power, Phys. Rev. B **80**, 233201 (2009).

[13] B. Wiendlocha, J.-B. Vaney, C. Candolfi, A. Dauscher, B. Lenoir, and J. Tobola, As Sn-induced resonant level in β-As_2Te_3, Phys. Chem. Chem. Phys. **20**, 12948 (2018).

[14] H. Wang, J. Hwang, C. Zhang, T. Wang, W. Su, H. Kim, J. Kim, J. Zhai, X. Wang, H. Park, *et al.*, Enhancement of the thermoelectric performance of bulk SnTe alloys via the synergistic effect of band structure modification and chemical bond softening, J. Mater. Chem. A **5**, 14165 (2017).

[15] M. Parzer, F. Garmroudi, A. Riss, S. Khmelevskyi, T. Mori, and E. Bauer, High solubility of Al and enhanced thermoelectric performance due to resonant states in Fe_2VAl_x, Appl. Phys. Lett. **120**, 071901 (2022).

[16] J. W. Simonson, D. Wu, W. J. Xie, T. M. Tritt, and S. J. Poon, Introduction of resonant states and enhancement of thermoelectric properties in half-Heusler alloys, Phys. Rev. B **83**, 235211 (2011).

[17] K. Vandaele, S. J. Watzman, B. Flebus, A. Prakash, Y. H. Zheng, S. R. Boona, and J. P. Heremans, Thermal spin transport and energy conversion, Mater. Today Phys. **1**, 39 (2017).

[18] S. J. Watzman, R. A. Duine, Y. Tserkovnyak, S. R. Boona, H. Jin, A. Prakash, Y. H. Zheng, and J. P. Heremans, Magnon-drag thermopower and Nernst coefficient in Fe, Co, and Ni, Phy. Rev. B **94**, 144407 (2016).

[19] Y. Zheng, T. Lu, M. M. H. Polash, M. Rasoulianboroujeni, N. Liu, M. E. Manley, Y. Deng, P. J. Sun, X. L. Chen, R. P. Hermann, *et al.*, Paramagnon drag in high thermoelectric figure of merit Li-doped MnTe, Sci. Adv. **5**, 1 (2019).

[20] M. M. H. Polash and D. Vashaee, Magnon-bipolar carrier drag thermopower in antiferromagnetic/ferromagnetic semiconductors: Theoretical formulation and experimental evidence, Phys. Rev. B **102**, 045202 (2020).

[21] W. Zhao, *et al.*, Superparamagnetic enhancement of thermoelectric performance, Nature **549**, 247 (2017).

[22] W. Zhao, Z. Liu, P. Wei, Q. Zhang, W. Zhu, X. Su, X. Tang, J. Yang, Y. Liu, J. Shi, *et al.*, Magnetoelectric interaction and transport behaviours in magnetic nanocomposite thermoelectric materials, Nat. Nanotechnol. **12**, 55 (2017).

[23] C. Li, S. Ma, P. Wei, W. Zhu, X. Nie, X. Sang, Z. Sun, Q. Zhang, and W. Zhao, Magnetism-induced huge enhancement of room-temperature thermoelectric and cooling performance of p-type BiSbTe alloys, Energ Environ. Sci. **13**, 535 (2020).

[24] S. Ma, C. Li, P. Wei, W. Zhu, X. Nie, X. Sang, Q. Zhang, and W. Zhao, High-pressure synthesis and excellent thermoelectric performance of Ni/BiTeSe magnetic nanocomposites, J. Mater. Chem. A **8**, 4816 (2020).

[25] C. P. Bean and J. D. Livingston, Superparamagnetism, J. Appl. Phys. **30**, S120 (1959).

[26] J. B. Vaney, S. A. Yamini, H. Takaki, K. Kobayashi, N. Kobayashi, and T. Mori, Magnetism-mediated thermoelectric performance of the Cr-doped bismuth telluride tetradymite, Mater. Today Phys. **9**, 100090 (2019).

[27] P. Cermak, P. Ruleova, V. Holy, J. Prokleska, V. Kucek, K. Palka, L. Benes, and C. Drasar, Thermoelectric and magnetic properties of Cr-doped single crystal Bi_2Se_3 – Search for energy filtering, J. Solid State Chem. **258**, 768 (2018).

[28] L. Zhao, C. Chen, L. Pan, X. Hu, C. Lu, and Y. Wang, Magnetic iron doping in Cu_2SnS_3 ceramics for enhanced thermoelectric transport properties, J. Appl. Phys. **125**, 095107 (2019).

[29] W. L. Xing, Z. C. Zhao, L. Pan, C. C. Chen, D. X. Li, and Y. F. Wang, Thermoelectric properties and magnetoelectric coupling in dually doped $Cu_2Sn_{1-2x}Zn_xFe_xS_3$, J. Mater. Sci.: Mater. Electron. **31**, 11801 (2020).

[30] F. Ahmed, N. Tsujii, and T. Mori, Thermoelectric properties of $CuGa_{1-x}Mn_xTe_2$: power factor enhancement by incorporation of magnetic ions, J. Mater. Chem. A **5**, 7545 (2017).

[31] R. Lu, J. S. Lopez, Y. Liu, T. P. Bailey, A. A. Page, S. Wang, C. Uher, and P. F. P. Poudeu, Coherent magnetic

nanoinclusions induce charge localization in half-Heusler alloys leading to high-*Tc* ferromagnetism and enhanced thermoelectric performance, J. Mater. Chem. A **7**, 11095 (2019).

[32] S. Acharya, S. Anwar, T. Mori, and A. Soni, Coupling of charge carriers with magnetic entropy for power factor enhancement in Mn doped $Sn_{1.03}Te$ for thermoelectric applications, J. Mater. Chem. C **6**, 6489 (2018).

[33] Z. C. Wei, C. Y. Wang, J. Y. Zhang, J. Yang, Z. L. Li, Q. D. Zhang, P. F. Luo, W. Q. Zhang, E. K. Liu, and J. Luo, Precise regulation of carrier concentration in thermoelectric BiSbTe alloys via magnetic doping, ACS Appl. Mater. Interfaces **12**, 20653 (2020).

[34] J. Kondo, Resistance minimum in dilute magnetic alloys, Prog. Theor. Phys. **32**, 37 (1964).

[35] J. Kondo, Giant thermo-electric power of dilute magnetic alloys, Prog. Theor. Phys. **34**, 372 (1965).

[36] Y. W. Shen, C. Li, R. Huang, R. M. Tian, Y. Ye, L. Pan, K. Koumoto, R. Z. Zhang, C. L. Wan, and Y. F. Wang, Eco-friendly *p*-type Cu_2SnS_3 thermoelectric material: crystal structure and transport properties, Sci. Rep. **6**, 32501 (2016).

[37] L. D. Zhao, G. J. Tan, S. Q. Hao, J. Q. He, Y. L. Pei, H. Chi, H. Wang, S. K. Gong, H. B. Xu, V. P. Dravid, *et al.*, Ultrahigh power factor and thermoelectric performance in hole-doped single-crystal SnSe, Science **351**, 141 (2016).

[38] X. X. Xu, H. W. Zhao, X. H. Hu, L. Pan, C. C. Chen, D. X. Li, and Y. F. Wang, Synergistic role of Ni-doping in electrical and phonon transport properties of $Cu_2Sn_{1-x}Ni_xS_3$, J. Alloy Compd. **728**, 701 (2017).

[39] H. W. Zhao, X. X. Xu, C. Li, R. M. Tian, R. Z. Zhang, R. Huang, Y. N. Lyu, D. X. Li, X. H. Hu, L. Pan, and Y. F. Wang, Cobalt-doping in Cu_2SnS_3: Enhanced thermoelectric performance by synergy of phase transition and band structure modification, J. Mater. Chem. A **5**, 23267 (2017).

[40] W. Zhou, P. Dwivedi, C. Shijimaya, M. Ito, K. Higashimine, T. Nakada, M. Takahashi, D. Mott, M. Miyata, M. Ohta, *et al.*, Enhancement of the thermoelectric figure of merit in blended $Cu_2Sn_{1-x}Zn_xS_3$ nanobulk materials, ACS Appl. Nano Mater. **1**, 4819 (2018).

[41] Z. Zhang, H. W. Zhao, Y. F. Wang, X. H. Hu, Y. N. Lyu, C. C. Cheng, L. Pan, and C. H. Lu, Role of crystal transformation on the enhanced thermoelectric performance in Mn-doped Cu_2SnS_3, J. Alloy Compd. **780**, 618 (2019).

[42] E. A. Pogue, M. Paris, A. Sutrisno, A. Lafond, N. Johnson, D. P. Shoemaker, and A. A. Rockett, Identifying short-range disorder in crystalline bulk Cu_2SnS_3 phases: A solid-state nuclear magnetic resonance spectroscopic investigation, Chem. Mater. **30**, 6624 (2018).

[43] Y. Wei, Z. Zhou, P. Jiang, S. Zheng, Q. Xiong, B. Zhang, G. Wang, X. Lu, G. Han, and X. Zhou, Phase composition manipulation and twin boundary engineering lead to enhanced thermoelectric performance of Cu_2SnS_3, ACS Appl. Energy Mater. **4**, 9240 (2021).

[44] K. Lohani, H. Nautiyal, N. Ataollahi, K. Maji, E. Guilmeau, and P. Scardi, Effects of grain size on the thermoelectric properties of Cu_2SnS_3: An experimental and first-principles study, ACS Appl. Energy Mater. **4**, 12604 (2021).

[45] See Supplemental Material at http://link.aps.org/supplemental/10.1103/PhysRevApplied.19.014034 for the experimental details, additional experimental data, details for DFT calculation [46–53], thermal conductivity calculations [2,54,55], and detailed results of TEM analysis [56,57].

[46] O. K. Andersen, Linear methods in band theory, Phys. Rev. B **12**, 3060 (1975).

[47] O. B. Jepsen and O. K. Andersen, *The TB-LMTO-ASA Program ver. 4.7* (MaxPlank-Institut fur Festkorperforschung, Stuttgart, Germany, 1999).

[48] G. Nam, W. Choi, H. Jo, K. M. Ok, K. Ahn, and T. S. You, Influence of thermally activated solid-state crystal-to-crystal structural transformation on the thermoelectric properties of the $Ca_{5-x}Yb_xAl_2Sb_6$ $(1.0 \leq x \leq 5.0)$ system, Chem. Mater. **29**, 1384 (2017).

[49] H. Sa, J. Lee, H. Jo, D. Moon, M. Kim, K. M. Ok, and T. S. You, *p*-type double doping and the diamond-like morphology shift of the Zintle phase thermoelectric materials: The $Ca_{11-x}A_xSb_{10-y}Ge_z$ (A = Na, Li; $0.06(3) \leq x \leq 0.17(5)$, $0.19(1) \leq y \leq 0.55(1)$, $0.13(1) \leq z \leq 0.22(1)$) system, Inorg. Chem. **60**, 10124 (2021).

[50] O. K. Andersen, O. Jepsen, and D. Glötzel, *Canonical description of the band structures of metals* (Highlights of Condensed Matter Theory, Elsevier North Holland, New York, 1985).

[51] O. A. Jepsen and O. K. Andersen, Calculated electronic structure of the sandwiched[1] metals LaI_2 and CeI_2: Application of new LMTO techniques, Phys. B **97**, 35 (1995).

[52] K. Momma and F. Izumi, VESTA 3 for three-dimensional visualization of crystal, volumetric and morphology data, J. Appl. Crystallogr. **44**, 1272 (2011).

[53] P. E. Blöchl, O. Jepsen, and O. K. Andersen, Improved tetrahedron method for Brillouin-zone integrations, Phys. Rev. B **49**, 16223 (1994).

[54] D. T. Morelli, J. P. Heremans, and G. A. Slack, Estimation of the isotope effect on the lattice thermal conductivity of group IV and group III-V semiconductors, Phys. Rev. B **66**, 195304 (2002).

[55] J. Zou and A. Balandin, Phonon hear conduction in a semiconductor nanowire, J. Appl. Phys. **89**, 2932 (2001).

[56] M. Onoda, X. A. Chen, A. Sato, and H. Wada, Crystal structure and twinning of monoclinic Cu_2SnS_3, Mater. Res. Bull. **35**, 1563 (2000).

[57] Von S. Strick, G. Eulenberger, and H. Hahn, Über einige quaternäre Chalkogenide mit Spinellstruktur, Z. Anorg. Allg. Chem. **357**, 338 (1968).

[58] M. Garst, P. Wolfle, L. Borda, J. von Delft, and L. Glazman, Energy-resolved inelastic electron scattering off a magnetic impurity, Phys. Rev. B **72**, 205125 (2005).

[59] A. C. Hewson, *The Kondo Problem to Heavy Fermions* (Cambridge University Press, UK, 1993).

[60] K. Yoshida, *Theory of Magnetism* (Springer-Verlag, Berlin-Heidelberg-New York, 1996), Vol. Solid-State Sciences 122.

[61] C. Kittel, *Introduction to Solid State Physics*, 7th ed. (John Wiley & Sons, New York, 1996).

[62] E. Borchi and S. D. Gennaro, Kondo effect in cerium intermetallics: Magnetic susceptibility, Phys. Rev. B **14**, 1989 (1976).

[63] S. Moris, P. Valencia-Galvez, J. Mejia-Lopez, O. Pena, P. Barahona, and A. Galdamez, $(Cu)_{tet}(Cr_{2-x}Sn_x)_{oct}S_{4-y}Se_y$: Crystal structure, density functional theory calculations, and magnetic behavior, Inorg. Chem. **58**, 13945 (2019).

[64] T. Ishikawa, S. Ebisu, and S. Nagata, Spin-glass and novel magnetic behavior in the spinel-type $Cu_{1-x}Ag_xCrSnS_4$, Phys. B: Condens. Matter **405**, 1881 (2010).

[65] B. A. E. Y. I. Ravich and I. A. Smirnov, *Semiconducting Lead Chalcogenides* (Plenum Press, New York-London, 1970).

[66] S. S. Li, *Semiconductor Physical Electronics* (Springer, 2006), Vol. 2.

[67] Y. T. Zhai, S. Y. Chen, J. H. Yang, H. J. Xiang, X. G. Gong, A. Walsh, J. Kang, and S. H. Wei, Structural diversity and electronic properties of Cu_2SnX_3 (X = S, Se): A first-principles investigation, Phys. Rev. B **84**, 075213 (2011).

[68] L. Xi, Y. B. Zhang, X. Y. Shi, J. Yang, X. Shi, L. D. Chen, W. Zhang, J. H. Yang, and D. J. Singh, Chemical bonding, conductive network, and thermoelectric performance of the ternary semiconductors Cu_2SnX_3 (X = S, Se) from first principles, Phys. Rev. B **86**, 155201 (2012).

[69] J. Pei, J. F. Dong, B. W. Cai, Y. Zhang, W. Zhou, B. P. Zhang, Z. H. Ge, and J. F. Li, Weak-ferromagnetism for room temperature thermoelectric performance enhancement in p-type $(Bi, Sb)_2Te_3$, Mater. Today Phys. **19**, 100423 (2021).

[70] D. P. Spitzer, Lattice thermal conductivity of semiconductors: A chemical bond approach, J. Phys. Chem. Solids **31**, 19 (1970).

[71] S. Lee, K. Esfarjani, T. F. Luo, J. W. Zhou, Z. T. Tian, and G. Chen, Resonant bonding leads to low lattice thermal conductivity, Nat. Commun. **5**, 3525 (2014).

[72] R. Hanus, M. T. Agne, A. J. E. Rettie, Z. W. Chen, G. J. Tan, D. Y. Chung, M. G. Kanatzidis, Y. Z. Pei, P. W. Voorhees, and G. J. Snyder, Lattice softening significantly reduces thermal conductivity and leads to high thermoelectric efficiency, Adv. Mater. **31**, 1900108 (2019).

[73] T. T. Deng, P. F. Qiu, Q. F. Song, H. Y. Chen, T. R. Wei, L. L. Xi, X. Shi, and L. D. Chen, Thermoelectric properties of non-stoichiometric $Cu_{2+x}Sn_{1-x}S_3$ compounds, J. Appl. Phys. **126**, 085111 (2019).